

A Unified GAN Framework Regarding Manifold Alignment for Remote Sensing Images Generation

Xingzhe Su · Wenwen Qiang · Zeen Song · Changwen Zheng ·
Fengge Wu · Fuchun Sun

Received: date / Accepted: date

Abstract Generative Adversarial Networks (GANs) and their variants have achieved remarkable success on natural images. However, their performance degrades when applied to remote sensing (RS) images, and the discriminator often suffers from the overfitting problem. In this paper, we examine the differences between natural and RS images and find that the intrinsic dimensions of RS images are much lower than those of natural images. As the discriminator is more susceptible to overfitting on data with lower intrinsic dimension, it focuses excessively on local characteristics of RS training data and disregards the overall structure of the distribution, leading to a faulty generation model. In respond, we propose a novel approach that leverages the real data manifold to constrain the discriminator and enhance the model performance. Specifically, we introduce a learnable information-theoretic measure to capture the real data manifold. Building upon this measure, we propose manifold alignment regularization, which mitigates the discriminator’s overfitting and improves the quality of generated samples. Moreover, we establish a unified GAN framework for manifold align-

ment, applicable to both supervised and unsupervised RS image generation tasks.

Keywords Image Generation · Generative Adversarial Networks · Remote Sensing · Data Manifold

1 Introduction

The image generation task (Xu and Jordan, 1996) is a fundamental problem in computer vision and has attracted significant attention from the research community. Various approaches have been proposed to address this challenge, including Generative Adversarial Networks (GANs), Variational Autoencoders, flow-based models, and so on. Among others, GANs (Goodfellow et al., 2014), in particular, have revolutionized the field by introducing a novel framework based on a zero-sum game between a generator and a discriminator. This framework has demonstrated remarkable success in generating realistic images. Since the introduction of GANs, they have become a cornerstone technique in various vision applications, such as image super-resolution (Ledig et al., 2017; Bell-Kligler et al., 2019; He et al., 2022), style transfer (Park et al., 2019; Wang et al., 2021; Richardson et al., 2021), and image editing (Ling et al., 2021; Patashnik et al., 2021; Pan et al., 2023).

Despite the remarkable success of current GAN methods, they still face various challenging problems, with the overfitting of the discriminator being a notable issue. The discriminator, equipped with an excessive number of parameters, can tend to memorize the training data rather than learning a meaningful distribution. This can result in a high real/fake classification accuracy on the training dataset but a lower accuracy on the validation split. When the discriminator becomes

Xingzhe Su, Wenwen Qiang, Zeen Song, Changwen Zheng,
Fengge Wu
Science & Technology on Integrated Information System Laboratory,
Institute of Software Chinese Academy of Sciences,
University of Chinese Academy of Sciences, Beijing, China

Fuchun Sun
Science & Technology on Integrated Information System Laboratory,
Department of Computer Science and Technology,
Tsinghua University, Beijing, China

Corresponding author: Wenwen Qiang, E-mail: qiangwenwen@iscas.ac.cn

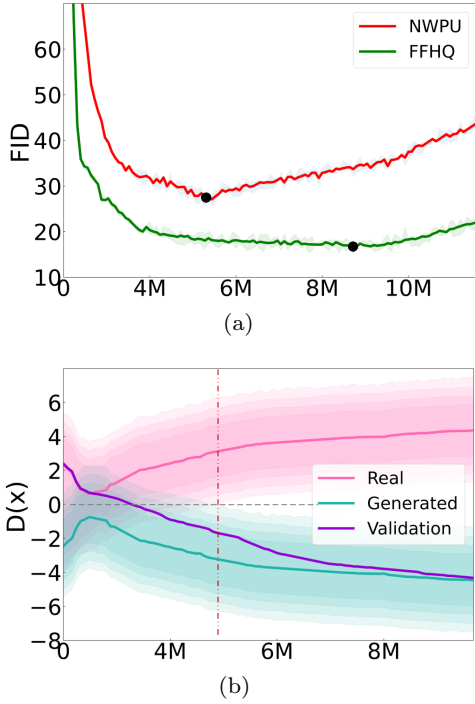


Fig. 1 The horizontal axis indicates the training process (the number of real images shown to the discriminator). (a) Training curves of StyleGAN2 on NWPU and FFHQ datasets. We randomly sample 30,000 training images from these two datasets, respectively. (b) The outputs of the discriminator during training on NWPU dataset.

overfit to the training samples, its feedback to the generator becomes less meaningful, leading to training divergence, excessive memorization, and limited generalization. Our experiments reveal that the overfitting problem of the discriminator is more pronounced when working with remote sensing (RS) data, as highlighted in Fig. 1. Specifically, we conducted the same experiment as outlined in (Karras et al., 2020a) on both the NWPU-RESISC45 and FFHQ256 datasets, maintaining the same training image size and dataset size for both. Notably, we observed that the GAN model diverged earlier when trained on RS data (Fig. 1(a)). Furthermore, Fig. 1(b) showcases the discriminator’s outputs during training, which align with the FID curves depicted in Fig. 1(a). The discernible drop in accuracy measured on a separate validation set further corroborates the overfitting problem of the discriminator specifically on the NWPU dataset. More experiment results can be found in the Appendix.

To identify possible causes, we analyze the differences between RS images and natural images in section 3.2. We find that the support of the distribution of RS data has lower dimension than that of natural images, implying that RS images can be embedded into lower-dimensional data manifold than natural

images. Intuitively, if the training dataset has lower-dimensional data manifold, the relationships between data samples could be simple, making the discriminator easier to overfit. To illustrate this issue, we perform a toy experiment on synthetic data in Section 3.2, as described in Fig. 3. The experiment clearly demonstrates that the discriminator becomes inclined to memorize the local characteristics of the training data while disregarding the global structure of the distribution during the training process. This behavior adversely affects the discriminator’s outputs and hinders the generator from effectively capturing the true data distribution, ultimately leading to a faulty generation model. Ideally, the discriminator should be capable of capturing the underlying manifold of both the training and generated data, and maximizing the difference between these two manifolds. This observation sheds light on potential solutions to mitigate the overfitting problem of the discriminator by applying manifold constraint. By imposing this constraint, we can urge the discriminator to focus on the underlying data manifold and limit the complexity of parameter space of the discriminator, thereby alleviating the overfitting problem.

In this paper, we propose a novel approach that leverages the real data manifold to mitigate the overfitting problem of the discriminator and enhance the quality of generated samples. Our methods neither entail heavy computational overheads nor require modifications of the network structure. Without loss of generality, an assumption that we will carry through our study is that the real datasets are not uniformly distributed in their ambient space, but are distributed over a union of low-dimensional nonlinear submanifolds. We first design a learnable information-theoretic measure to evaluate the intrinsic geometric of the training samples. Then we propose novel regularization terms based on this measure in loss functions of GAN models, which we call manifold alignment constraint (MAC). The MAC encourages the discriminator to misalign the manifold of the generated samples with that of the real images, thereby focusing on the underlying data manifold of the real images and reducing the complexity of the discriminator’s parameter space. On the other hand, the generator aims to align the manifold of the generated samples with that of the real images, effectively capturing the intrinsic characteristics of the real data and improving the overall performance of the generative model. We theoretically and empirically prove the efficacy of MAC in manifold alignment during GAN training. Finally, we establish a unified GAN framework for supervised and unsupervised RS images generation. In summary, the contributions of this paper are the following:

- We empirically demonstrate that RS images have lower-dimensional data manifold than natural images, which leads to the discriminator easily overfitting to the RS training distribution, neglecting the underlying data manifold.
- We propose an information-theoretic measure to evaluate the difference between the real and generated data manifolds, which helps constrain the discriminator and enhance the performance of the generator.
- We design novel learning paradigms under supervised and unsupervised settings, and establish a unified GAN framework for supervised and unsupervised RS images generation.
- We theoretically and empirically prove the efficacy of our method. Extensive experiments on three RS datasets and three natural datasets validate the versatility of our approach.

2 Related Work

Generative adversarial networks. GANs are notorious for training instability and mode collapse. Various adversarial losses have been proposed to stabilize the training or improve the convergence of the GAN models (Goodfellow et al., 2014; Mroueh and Sercu, 2017; Arjovsky et al., 2017). Additionally, numerous efforts have been made to address this issue using regularization methods (Mescheder et al., 2018; Miyato et al., 2018; Gulrajani et al., 2017; Srivastava et al., 2017), or modifying network architectures (Zhang et al., 2019a; Brock et al., 2018; Karras et al., 2019, 2020b; Esser et al., 2021; Jiang et al., 2021b; Metz et al., 2017). Other than these problems, the overfitting of the discriminator is also a common challenge in GANs.

The overfitting problem occurs when the discriminator becomes overly complex with a large number of parameters, resulting in memorization of the training data rather than learning the underlying data distribution. This leads to poor generalization and a lack of diversity in generated samples, particularly when the training dataset is limited. Recent methods (Zhang et al., 2019b; Jiang et al., 2021a; Zhao et al., 2020; Karras et al., 2020a) have tackled this issue by leveraging data augmentation techniques to increase data diversity and prevent overfitting. Other than data augmentation, regularization methods such as Lecam (Tseng et al., 2021) have been proposed to enhance the generalization of GAN models trained on limited data. InsGen (Yang et al., 2021) proposes a contrastive learning objective to enhance the adversarial loss in the few-shot generation setting. MoCA (Li et al., 2022) proposes prototype-based memory modulation module to improve the gen-

erator network of a GAN. FastGAN (Liu et al., 2020) introduces a self-supervised discriminator and a Skip-Layer channel-wise Excitation (SLE) module for efficient few-shot image synthesis. However, these methods primarily focus on the general distribution of the training data and do not explicitly consider the real data manifold.

Previous works (Park et al., 2017; Li et al., 2018) introduce geometry constraints to GANs loss functions. These methods utilize statistical mean and radius to approximate the geometry of the real data, but they may lack accurate constraints on the data manifold and may lose important geometrical information. Other approaches (Ni et al., 2022; Bang and Shim, 2021; Khayatkhoei et al., 2018) require auxiliary networks to map the generated data into the submanifolds of the real data. In this paper, we focus on intrinsic dimensions of training images, and minimizing distance between real and synthetic data in the feature space. Our methods do not introduce heavy computational overhead or require modifications to the network structure.

GAN in the RS field. In this paper, we focus on RS RGB images. Existing GAN models in the RS field can be divided into two types according to their applications. This first kind is augmenting training samples (Lin et al., 2017; Yu et al., 2019; Wei et al., 2020; Chen et al., 2021). The second kind deals with image-generation-related tasks such as image translation (Bjiga et al., 2020; Rui et al., 2021; Chen et al., 2020; Zhao et al., 2021) and image super-resolution (Jiang et al., 2019; Xiong et al., 2020). However, these methods do not delve into the characteristics of RS images, and the generated images are of low quality. In this paper, we explore the intrinsic dimensions of RS images, and introduce RS data manifold constraints in the loss functions. Note that this is the first work to focus on the manifold alignment on RS image generation tasks.

3 Preliminary Study and Analysis

In this section, we first introduce the basic framework of GANs. Then we explore the differences between RS images and natural images. Finally, we analyze plausible reasons about the poor results of the GAN models on RS images and derive the motivation for this paper.

3.1 Preliminary GANs

The GAN model aims to learn the distribution of training samples. Based on the idea of the zero-sum game, a GAN model consists of a generator G and a discriminator D . The generator aims to generate realistic samples

to fool the discriminator, while the discriminator tries to distinguish between real and fake samples. When the model reaches the final equilibrium point, the generator will model the target distribution and produce counterfeit samples, which the discriminator will fail to discern. Let \mathcal{V}_D and \mathcal{V}_G denote the training objectives of the discriminator D and the generator G , respectively. The training of the GAN frameworks can be generally illustrated as follows:

$$\max_D \mathcal{V}_D = \mathbb{E}_{x \sim P_{\text{data}}} [D(x)] - \mathbb{E}_{z \sim p_z} [D(G(z))] \quad (1)$$

$$\max_G \mathcal{V}_G = \mathbb{E}_{z \sim p_z} [D(G(z))] \quad (2)$$

where the input vector z of G is usually sampled from the *normal distribution*.

3.2 Problem Analysis and Motivations

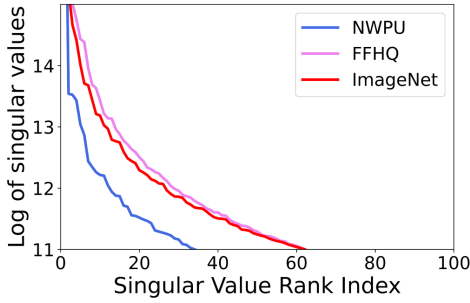


Fig. 2 Singular value decomposition on RS images and natural images in sorted order and logarithmic scale.

As we mentioned above, current GAN methods often suffer from the overfitting problem of the discriminator, as shown in Fig.1. In order to identify the plausible causes, we analyze the differences between RS images and natural images.

We randomly sample 10,000 images from the NWPU dataset and convert these images to grayscale. We convert the images to one-dimensional vector, denoted as $X = [x_1, x_2, \dots, x_N]$, where the vector x_i concatenates all pixels of an image. Then, we get the average vector $\bar{x} = \frac{1}{N} \sum_{i=1}^N x_i$. We calculate $\hat{x}_i = x_i - \bar{x}$ and get $\hat{X} = [\hat{x}_1, \hat{x}_2, \dots, \hat{x}_N]$. Fig.2 shows singular value decomposition on the matrix $M = \hat{X}\hat{X}^T$ ($M = USV^T$, $S = \text{diag}(\sigma^k)$) in sorted order and logarithmic scale ($\{\log(\sigma^k)\}$). We perform the same experiment on FFHQ dataset and ImageNet dataset as shown in Fig.2. The singular values commonly correspond to important information implied in the matrix, and the importance is positively related to the magnitude of the singular value. We observe that the singular values of RS images

are smaller than those of natural images, and there are fewer singular values with relatively large magnitudes of RS images compared with natural images. Thus, we conclude that the support of the distribution of RS data has lower dimension than those of natural images in the input space.

Based on our empirical findings above, RS images are distributed on lower-dimensional manifold than natural images. Intuitively, if the training data has a high-dimensional data manifold, the discriminator must learn a more complex decision boundary to distinguish between real and fake samples. This can make it more difficult for the discriminator to overfit to the training data, as it must learn a more generalized representation of the data distribution. In contrast, as depicted in Fig.3, when the training data has a low-dimensional data manifold, such as the swiss roll-shaped manifold illustrated in Fig.3(a), the discriminator can more easily memorize the training data and overfit to the limited variations within the data. Without sufficient training samples, the discriminator tends to neglect the real data manifold and produces biased outputs. Consequently, the generator fails to learn the true data manifold, resulting in a faulty generative model, as depicted in Fig.3(b).

The optimal discriminator should be able to capture the underlying manifold of training data and generated data, and maximize the difference between these two manifolds. Inspired by the observation, we propose applying a manifold constraint on the discriminator. In this way, we can guide the discriminator to focus on the underlying data manifold, which helps limit the complexity of the discriminator’s parameter space and alleviate the overfitting problem. Furthermore, by ensuring the alignment between the manifold of generated samples and the real data manifold, the generator can effectively learn the intrinsic structure of the real data. This alignment enhances the quality and diversity of the generated samples, leading to improved performance (Fig.3(c)).

In practice, it is intractable to learn the data manifold in the high-dimensional ambient space \mathbb{R}^D . Be aware that we assume the data x is distributed over a union of low-dimensional nonlinear submanifolds $\cup_{j=1}^k \mathcal{M}_j \subset \mathbb{R}^D$, where each submanifold \mathcal{M}_j is of dimension $d_j \ll D$. Given this assumption, the images from each submanifold $\mathcal{M}_j \subset \mathbb{R}^D$ can be mapped to a linear subspace $\mathcal{S}_j \subset \mathbb{R}^d$, which we call the feature space. It is easier to evaluate the structure of the representations of images in the feature space, which also reflects the data manifold in image space. Consequently, the representations of images should have following properties:

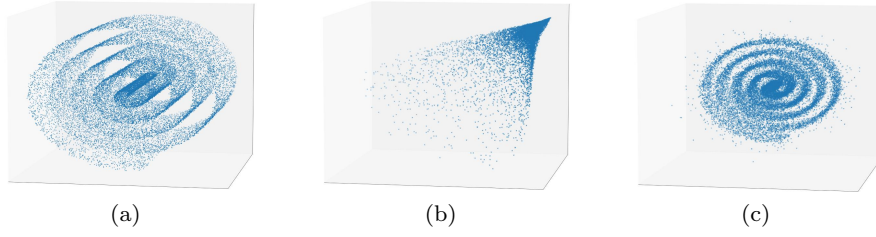


Fig. 3 (a) Real data manifold. (b) Data manifold of generated images. (c) Data manifold of generated images by applying manifold constraint.

- Between-Mode Uniformity: Representations from different modes or classes should be highly uncorrelated.
- Within-Mode Similarity: Representations from the same mode or class should be relatively correlated.
- Maximally Variance: Representations should have as large dimension as possible to cover all the modes or classes and be variant for the same mode or class.

In order to obtain qualified representations, we need a new measure to evaluate the goodness of the resulting representations in terms of all these properties. In respond, we propose a novel information-theoretic measure, and design new regularization terms regarding the manifold alignment of RS images, which will be elaborated below.

4 Methods

In this section, we first introduce the new information-theoretic measure to evaluate the intrinsic geometric of the distribution of features. Then we design novel regularization terms based on this measure, which we call manifold alignment constraint (MAC). We theoretically and empirically prove the efficacy of MAC in manifold alignment on GAN training. Finally, we establish a unified GAN framework for supervised and unsupervised RS images generation as shown in Fig.4. Next, we will introduce in detail.

4.1 Manifold Alignment Constraint

The key idea in this paper is to find a principled measure which could accurately and directly represent intrinsic geometric or statistical properties of the distribution. To achieve this, we turn to information theory, which suggests that the uniform distribution contains the most information and has the maximum information entropy. From this perspective, a more dispersed distribution indicates more information, whereas a more compact distribution indicates less information.

We can therefore evaluate the information contained in the features to represent their intrinsic geometric properties. Building on this intuition, we could design a measure of compactness for the distribution of a random variable or from its finite samples.

Notably, the singular vectors associated with larger singular values represent the dominant stretching directions in the data. Consequently, larger singular values and a greater number of large singular values correspond to more scattered data, while smaller singular values and fewer large singular values signify more compact data. Thus we propose to use $\sum_{i=1} \lambda_i^2$ to evaluate the compactness of the distribution of features, where λ_i denotes the singular value. As the square of the Frobenius norm of the matrix M equals to the sum of the squares of the singular values. Meanwhile, the square of the Frobenius norm equals to the trace of MM^T . Thus, we use the trace of MM^T in our experiments.

$$\sum_{i=1} \lambda_i^2 = \|M\|_F^2 = \text{Tr}(MM^T) \quad (3)$$

where λ_i is singular value and Tr is the trace operator.

To ensure between-mode uniformity, it is desirable that features of different modes or classes are maximally uncorrelated with each other. Therefore, they together should span a space of the largest possible volume or dimension, and the Frobenius norm of the whole set Z should be as large as possible. Conversely, learned features of the same mode or class should be highly correlated and coherent. Therefore, each mode or class should only span a space or subspace of a very small volume, and the Frobenius norm should be as small as possible. To evaluate whether the representation of images satisfy the three properties mentioned above, we design a novel measure based on Eq.3.

$$\mathcal{L}_{\text{Tr}}(Z) = \frac{1}{2n} \left(\text{Tr}(ZZ^T) - \sum_{j=1}^k \text{Tr}(ZC^jZ^T) \right) \quad (4)$$

where $Z = [z_1, \dots, z_n] \in \mathbb{R}^{d \times n}$ denotes the representations of images, $C = \{C^j \in \mathbb{R}^{n \times n}\}_{j=1}^k$ is a set of

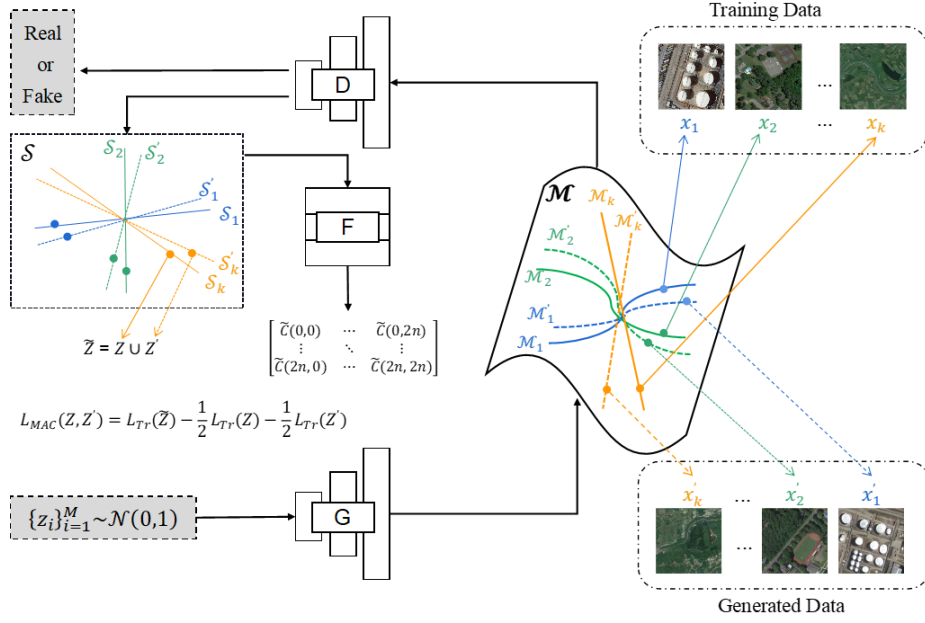


Fig. 4 The overall architecture of our method. G and D are generator and discriminator. F is the MLP network for relationship matrix C . \mathcal{M} is manifold, and \mathcal{S} is feature space. This figure only denotes the unsupervised generation process for simplicity.

positive diagonal matrices whose diagonal entries denote the membership of the n samples in the k classes. In the supervised setting, k is the number of classes. If the sample i belongs to the mode or class j , then $C^j(i, i) = 1$. Otherwise, $C^j(i, i) = 0$. In the unsupervised setting, we provide a novel learning paradigm for matrix C^j , which will be elaborated in the next section.

By maximizing the first term of \mathcal{L}_{Tr} , we aim to encourage a uniform distribution across the entire set of images. On the other hand, by minimizing the second term of \mathcal{L}_{Tr} , we intend to enforce compactness within the distribution of generated images that belong to the same mode or class. By balancing these two terms, we could force the distributions of the generated images belonging to different modes or classes to be dispersed. Consequently, the representations of generated images satisfy the three conditions mentioned above, which in turn ensures the generated images are distributed over a union of low-dimensional nonlinear submanifolds. However, this constraint alone is insufficient, and we also need to evaluate the disparity of the submanifolds between generated images and real images. Inspired by mutual information, we design the following measure:

$$\mathcal{L}_{MAC}(Z, Z') = \mathcal{L}_{Tr}(Z, Z') - \frac{1}{2} \mathcal{L}_{Tr}(Z) - \frac{1}{2} \mathcal{L}_{Tr}(Z') \quad , \quad (5)$$

where Z denotes the representations of real images, while Z' is the representations of generated images. $\mathcal{L}_{Tr}(Z, Z') = \frac{1}{2n} (\text{Tr}(\tilde{Z}\tilde{Z}^T) - \sum_{j=1}^k \text{Tr}(\tilde{Z}\tilde{C}^j\tilde{Z}^T))$, where $\tilde{Z} = Z \cup Z'$, $\tilde{C}^j \in \mathbb{R}^{2n \times 2n}$. In the supervised setting, if the sample i belong to the mode or class j , then

$C^j(i, i) = 1, C^{j'}(i, i) = 1, \tilde{C}^j(i, i) = 1$. In the unsupervised setting, $C^j, C^{j'}$ and \tilde{C}^j are all learnable matrices.

We theoretically prove that the above quantity precisely measures the volume of the space between Z and Z' . The proof will be elaborated in the next section. By maximizing the MAC, the discriminator is encouraged to push the manifold of the generated samples to be misaligned with that of the real images. On the other hand, by minimizing the MAC, the generator aims to align the manifold of the generated samples with that of the real images. Based on Eq.5, we refine the loss functions of GAN models regarding manifold alignment and establish a unified GAN framework for supervised and unsupervised RS images generation.

4.2 Loss Functions

We incorporate the manifold alignment constraint (MAC) as regularization terms in the loss functions of GAN models, as depicted in Eq.6 and Eq.7, where λ and γ are hyperparameters. The representations Z and Z' are learned by the discriminator.

$$\min_D \mathcal{L}_D = \mathbb{E}_{z \sim p_z} [D(G(z))] - \mathbb{E}_{x \sim P_{\text{data}}} [D(x)] - \lambda \mathcal{L}_{MAC}(Z, Z') \quad (6)$$

$$\min_G \mathcal{L}_G = - \mathbb{E}_{z \sim p_z} [D(G(z))] + \gamma \mathcal{L}_{MAC}(Z, Z') \quad (7)$$

Supervised. For the generator, we use the same architecture as previous models and add the label in-

formation as additional input. However, for the discriminator, we do not use the label information directly as previous class-conditional models. Instead, we incorporate the MAC to ensure that the generated images align with the classes of real images. The $C^j(i, i)$ in MAC denotes the relationship of sample i and class j , and $C^j(i, i) = 1$ means that the sample i belongs to the mode or class j . Additionally, we add a fully connected layer at the final block of the discriminator as an extra branch to learn representations Z , which is incoherent to the original unconditional output.

Unsupervised. For the unsupervised setting, the relationship matrix C and representations Z have various implementations. For the matrix $C = \{C^j \in \mathbb{R}^{n \times n}\}_{j=1}^k$, we design a novel learning paradigm. Specifically, we set $k = n$ and learn a matrix C^j for each sample j . We train a three-layer MLP network F to learn the relationship between sample i and sample j in the feature space. Hence, $C^j(i, i) = F(z_i, z_j)$, where z_i and z_j are representations of sample x_i and sample x_j , respectively. Then, we use a pretrained encoders f_{pre} to obtain the prior feature representations, denoted as $\bar{Z} = \{\bar{z}_1, \dots, \bar{z}_n\}$, where $\bar{z}_i = f_{\text{pre}}(x_i)$, $i \in \{1, \dots, n\}$. Then, regarding the j -th element \bar{z}_j in \bar{Z} as the anchor, we define that:

$$C^{j_{\text{pro}}}(i, i) = \exp(\|\bar{z}_i - \bar{z}_j\|_2^2 / \tau) \quad (8)$$

where \bar{z}_i is the i -th sample in \bar{Z} . Then, we can obtain:

$$C^{j_{\text{pro}}} = [\bar{C}^{j_{\text{pro}}}(1, 1), \dots, \bar{C}^{j_{\text{pro}}}(n, n)] \quad (9)$$

where $\bar{C}^{j_{\text{pro}}}(k, k) = C^{j_{\text{pro}}}(k, k) / \sum_{h=1}^n C^{j_{\text{pro}}}(h, h)$. We in turn treat the samples in \bar{z}_i as anchors and obtain $C^{j_{\text{pro}}} = [C^{1_{\text{pro}}}, \dots, C^{n_{\text{pro}}}]^T$. To this end, we give the prior constraint $C^{j_{\text{pro}}}$ of C based on a pre-trained encoder and the Euclidean distance of different pairs of samples. Since $C = F(Z)$, the loss function of network F is as follows:

$$\mathcal{L}_{\text{con}} = \beta \|C^{j_{\text{pro}}} - F(Z)\|_2^2 \quad (10)$$

The network F is trained together with the discriminator, β is the hyperparameter. In the optimal case, the network F will learn the relationship between the samples, and $F(z_i, z_j) = 1$ if sample x_i and sample x_j are from the same mode or class. In our experiments, we find that the choice of the pre-trained encoder has no impact on the final results.

For the representations Z , it has been shown that different network layers are responsible for different levels of detail in the images. Empirically, the latter blocks of the network have more effect on the style (e.g. texture and color) of the image whereas the earlier blocks impact the coarse structure or content of the image

(Patashnik et al., 2021). Thus, we choose features from a shallow network layer of the discriminator as representations Z in our experiments.

5 Theoretical and Empirical Analysis

In this section, we present theoretical and empirical analysis of the proposed method, MAC. Firstly, we establish a theoretical connection between our method and information theory, and prove that the proposed method can precisely measure the distance between generated images and real images in the feature space. Secondly, we conduct two toy experiments on synthetic data to demonstrate the effectiveness of our approach empirically.

5.1 Theoretical Analysis

This section provides provability results and properties of our method. First, we prove the theoretical connection between our method and information theory. Then, we prove our method can precisely measure the distance between generated images and real images in the feature space.

Proposition 1 $\frac{1}{2n} \text{Tr}(ZZ^T)$ where $Z = [z^1, \dots, z^n] \subset \mathbb{R}^{d \times n}$ can measure the compactness of a distribution from its finite samples Z .

Proof Based on the first-order Taylor series approximation, $\log \det(\mathbf{C} + \mathbf{D}) \approx \log \det(\mathbf{C}) + \text{Tr}(\mathbf{D}^T \mathbf{C}^{-1})$, we can get following equations.

$$\begin{aligned} \frac{1}{2n} \text{Tr}(ZZ^T) &= \frac{1}{2} \left(\frac{1}{n} \text{Tr}(ZZ^T) + \log \det(\mathbf{I}) \right) \\ &\approx \frac{1}{2} \log \det\left(\mathbf{I} + \frac{1}{n} ZZ^T\right) \end{aligned}$$

In information theory, rate distortion can be used to measure the ‘‘compactness’’ of a random distribution (Cover and Thomas, 2006). Given a random variable z and a prescribed precision $\epsilon > 0$, the rate distortion $R(z, \epsilon)$ is the minimal number of binary bits needed to encode z such that the expected decoding error is less than ϵ . Given finite samples $Z = [z^1, \dots, z^m] \subset \mathbb{R}^{d \times m}$, the total number of bits needed is given by the following expression: $\mathcal{L}(Z, \epsilon) \doteq \left(\frac{m+d}{2}\right) \log \det\left(\mathbf{I} + \frac{d}{m\epsilon^2} ZZ^T\right)$. As the sample size m is large, our approach can be seen as an approximation of the code rate distortion, which completes our proof.

Based on the above derivation, the proposed measure can be rewritten as:

$$\mathcal{L}_{\text{Tr}} \approx \frac{1}{2} \log \det (\mathbf{I} + \alpha \mathbf{Z} \mathbf{Z}^T) - \sum_{j=1}^k \frac{\gamma_j}{2} \log \det (\mathbf{I} + \alpha_j \mathbf{Z} \mathbf{C}^j \mathbf{Z}^T) \quad (11)$$

where $\alpha = \frac{d}{n\epsilon^2}$, $\alpha_j = \frac{d}{\text{Tr}(\mathbf{C}^j)\epsilon^2}$, $\gamma_j = \frac{\text{Tr}(\mathbf{C}^j)}{n}$ for $j = 1, \dots, k$.

Therefore, our method \mathcal{L}_{Tr} can measure the volume of the space spanned by representations, making it an effective method to promote embedding of data into multiple independent subspaces. Since the features of each mode or class, \mathbf{Z}_j and \mathbf{Z}'_j , are similar to subspaces or Gaussians, their “distance” can be measured by the rate distortion. Hence, our method $\mathcal{L}_{\text{MAC}}(\mathbf{Z}, \mathbf{Z}')$ can precisely measure the distance between generated images and real images in the feature space.

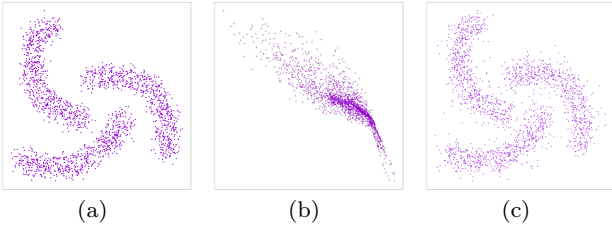


Fig. 5 (a) Ground truth. (b) Data generated by original GAN. (c) Data generated by our method.

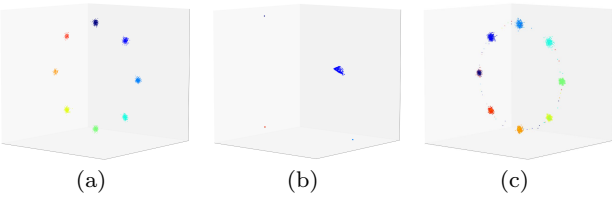


Fig. 6 (a) Ground truth. (b) Data generated by original GAN. (c) Data generated by our method.

5.2 Empirical Analysis

To demonstrate the effectiveness of our proposed method on GAN training, we conduct two toy experiments on synthetic data. In the first experiment, we generated synthetic data points that are uniformly distributed on three vortex lines (Fig.5(a)). We train the original GAN architecture without and with our

method for 10,000 iterations, and the results are shown in Fig.5(b) and Fig.5(c), respectively. From the comparison in the figure, it is clear that the original GAN fails to capture the three modes, while our proposed method evenly spreads the probability mass and captures all three modes of the training data.

The second experiment is supervised generation on a 2D mixture of eight Gaussians evenly arranged in a circle. Moreover, the circle of the Gaussian mixture lies in a hyperplane in a 3D space (Fig.6(a)). Therefore, the generator has to search for 2D submanifolds in a 3D space. We present the results of the original CGAN in Fig.6(b) and our proposed method in Fig.6(c), both trained for 10,000 iterations. From the comparison in the figure, it is clear that the original CGAN only learns one mode, while our proposed method evenly spreads the probability mass and converges to all eight modes. Additionally, we observe that the data mass generated by our proposed method is heavily concentrated within the mode, whereas the data mass generated by the original CGAN scatters around the mode.

6 Experiments

In this section, we first provide the details of our experimental setup. We use three remote sensing datasets to evaluate our method: the UC Merced Land Use Dataset (Yang and Newsam, 2010), NWPU-RESISC45 Dataset (Gong et al., 2017) and PatternNet Dataset (Zhou et al., 2018). Details of these datasets can be found in the appendix. We also conduct experiments on three natural datasets: FFHQ256 Dataset (Karras et al., 2019), LSUN-cat Dataset (Yu et al., 2015) and Cifar10 Dataset (Krizhevsky and Hinton, 2009). We present the quantitative and qualitative results of the proposed method, as well as the comparison with existing methods. Finally, we provide more ablation and analysis of different components of our method.

6.1 Experiment Setup

Implementation details: For unsupervised generation, we base our method on two different models **StyleGAN2** (Karras et al., 2020b) and **BigGAN** (Brock et al., 2018) with different augmentation methods **ADA** (Karras et al., 2020a) and **APA** (Jiang et al., 2021a), and regularization method **LeCam** (Tseng et al., 2021). We also compare our method with few-shot generation models **FastGAN** (Liu et al., 2020), **InsGen** (Yang et al., 2021) and **MoCA** (Li et al., 2022). We use the official PyTorch implementation of StyleGAN2+ADA, FastGAN, InsGen and Style-

GAN2+MoCA. For BigGAN, APA and LeCam, we use the implementations provided by (Kang and Park, 2020). For class-conditional generation, we base our method on TC-GAN (Shahbazi et al., 2022). We compare our method with MSGAN (Mao et al., 2019), TC-GAN (Shahbazi et al., 2022), DivCo (Liu et al., 2021), ContraGAN (Kang and Park, 2020), conditional BigGAN and StyleGAN2. We use the official PyTorch implementation of these methods. We set $\lambda = 1$, $\gamma = 1$, and $\beta = 1$ in our experiments, and the ablation study on these hyperparameters are available in the Appendix.

Evaluation Metrics: We evaluate our method using Frechet inception distance (FID) (Heusel et al., 2017), as the most commonly-used metric for measuring the quality and diversity of images generated by GAN models. We also include Kernel Inception Distance (KID) (Bińkowski et al., 2018) as a metric that is unbiased by empirical bias (Xu et al., 2018).

6.2 Unsupervised Generation

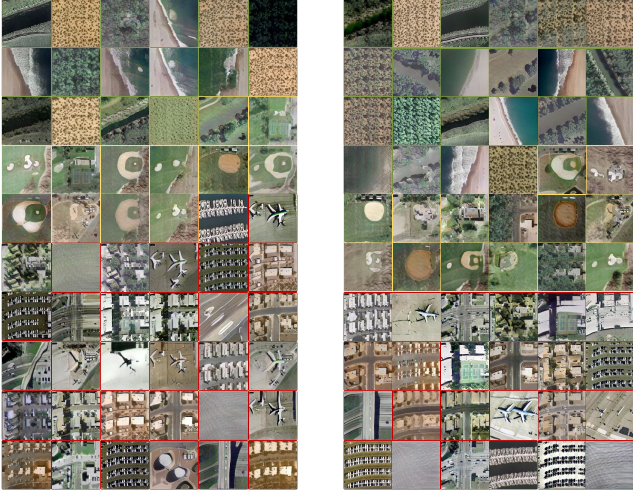


Fig. 7 Experiment results of unsupervised generation on the UCLand Dataset. The colors of image border become warmer with increasing artificial landscapes (Green→Yellow→Red). The generated images of StyleGAN2(left) are uneven with more natural landscapes. In contrast, our method(right) has a more even distribution of generated images.

We first visualize the generated images of our method in Fig.7. We run the models for 5 times and select the categories with higher occurrences. In comparison to StyleGAN2, our method produces a more even distribution of natural and artificial landscapes. The training curve of our method (based on StyleGAN2) on NWPU dataset is shown in Fig.8(a), and Fig.8(b)

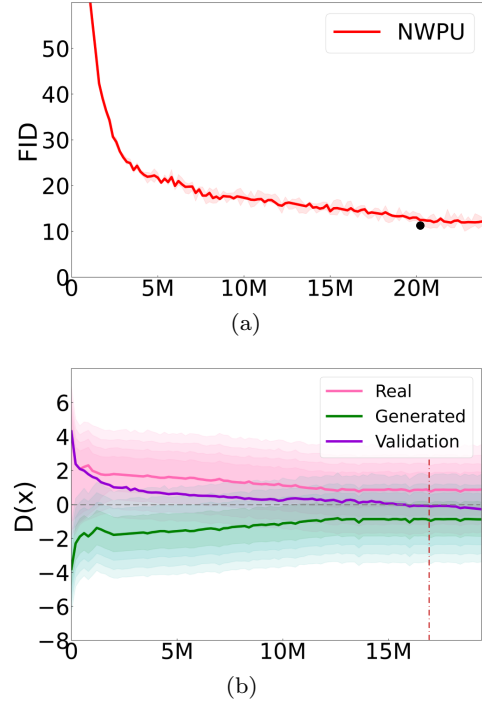


Fig. 8 The horizontal axis indicates the training process (the number of real images shown to the discriminator). (a) Training curves of our method on NWPU dataset. (b) The outputs of the discriminator during training.

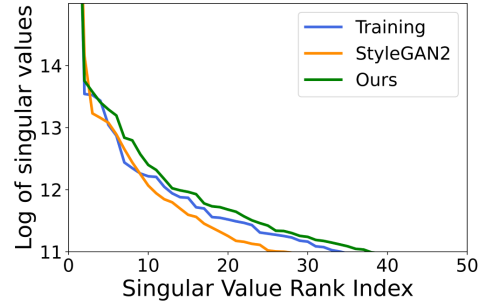


Fig. 9 Singular value decomposition on training images, generated images by StyleGAN2, and generated images by our method in sorted order and logarithmic scale.

is the output of the discriminator during training. We can observe that the overfitting problem of the discriminator is alleviated. We also conduct a similar experiment in Section 3.2 on NWPU dataset. Specifically, we compare the singular values of the images generated by StyleGAN2 and our proposed method. The results are depicted in Figure 9, and they clearly demonstrate that our method, which incorporates the manifold constraint, enables the discriminator to focus on the underlying data manifold and capture its essential characteristics. As a result, the images generated by our method exhibit more effective and meaningful informa-

Table 1 Comparison of Quality Scores (FID↓, KID↓) on the UCLand, NWPU-RESISC45 and PatternNet Dataset (the red numbers present our improvement)

Methods	UCLand		NWPU		PatternNet	
	FID	KID	FID	KID	FID	KID
BigGAN+ADA	98.09- 5.92	52.31- 4.24	30.91- 3.39	11.13- 1.85	63.94- 3.59	36.71- 1.63
BigGAN+ADA+LeCam	92.52- 5.27	48.59- 3.52	32.65- 2.57	12.69- 1.87	54.28- 4.42	25.89- 2.37
StyleGAN2	89.33- 12.27	45.39- 8.79	27.52- 11.29	10.71- 6.03	42.93- 9.84	20.11- 5.97
StyleGAN2+APA	78.54- 4.39	39.25- 3.79	21.67- 2.78	8.54- 2.03	33.75- 4.84	13.34- 2.99
StyleGAN2+ADA	74.25- 4.82	37.08- 4.08	11.97- 2.09	3.27- 0.92	33.53- 3.06	13.67- 2.32
StyleGAN2+ADA+LeCam	70.89- 3.91	32.21- 2.86	14.38- 2.34	4.97- 1.47	25.87- 2.86	9.32- 1.73

Table 2 Comparison of Quality Scores (FID↓) on the UCLand, NWPU-RESISC45 and PatternNet Dataset

Methods	UCLand	NWPU	PN
FastGAN	76.63	32.17	51.39
InsGen	95.65	10.92	50.76
MoCA	71.25	10.37	32.79
Ours	69.43	9.88	30.47

tion. Additional visual results and experiments on other datasets are available in the Appendix.

Then, we provide a quantitative comparison with the well-established baselines. Results are reported in Table 1 and Table 2. The red numbers in Table 1 indicate the improvement of the GAN models after using our method. In general, the FID and KID scores for our proposed method indicate a significant and consistent advantage over all the compared methods. In detail, our comparison experiments can be divided into three types. First, under different model structures, BigGAN and StyleGAN2, our method is robust, which proves that our approach can be applied to any model architecture. Second, under different augmentation methods, ADA and APA, our method still performs well. This shows that the proposed approaches can be applied to other GAN models along with existing augmentation approaches. Third, combined with the regularization method LeCam, our method is still effective. The proposed method can be viewed as an effective complement to existing regularization methods. Furthermore, we conduct a comparative analysis between our method and existing few-shot generation methods, as showcased in Table 2. Given the severity of the overfitting problem in few-shot generation tasks, it is crucial to compare the performance of our approach with these methods. In our experiments, InsGen, MoCA and our method are all implemented based on StyleGAN2+ADA. The results in Table 2 clearly demonstrate that our method consistently outperforms the existing methods, further highlighting its effectiveness in addressing the overfitting challenge. Other than

Table 3 Experiment Results on Three Natural Datasets

Method	FFHQ(FID↓)		Cat(FID↓)		Cifar10(IS↑)	
	10k	2k	30k	5k	UG	CG
Baseline	9.62	20.36	12.87	25.97	9.41	9.72
Ours	8.41	17.81	11.77	23.52	9.88	10.19

RS datasets, we also conduct experiments on three natural datasets: FFHQ256 Dataset, LSUN-cat Dataset and Cifar10 Dataset. The results are shown in Table 3, and we use the StyleGAN2+ADA as the baseline. We use Inception Score (IS) (Salimans et al., 2016) as image quality metric on Cifar10 for better comparison with previous works. "UG" and "CG" represent unsupervised generation and conditional generation, respectively. These experiments validate the efficacy of our approach on different datasets.

To further assess the discriminator’s ability to capture the underlying data manifold, we perform unsupervised classification experiments on the UC-Merced and NWPU-RESISC45 datasets. In these experiments, we utilize the learned representations Z as features and employ a regularized linear L2-SVM classifier, following the methodology employed in previous studies Lin et al. (2017) Yu et al. (2019). The experimental results, presented in Table 4, clearly demonstrate the superior performance of our method compared to StyleGAN2+ADA across all tests. Our approach consistently achieves the best results in the majority of the experiments, which proves that our method is capable of learning improved representations that facilitate accurate data classification. These experiments provide further confirmation that by applying the manifold constraint, the discriminator is able to focus on the underlying data manifold and capture its essential characteristics.

6.3 Class-conditional Generation

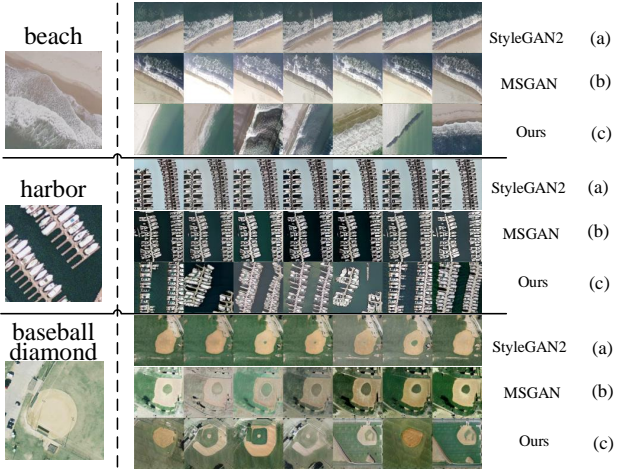
We first present the generated images of class-conditional experiment in Fig.10. Unlike previous class-

Table 4 Comparison of Unsupervised Classification Accuracy(%) on the UC-Merced Dataset and NWPU-RESISC45 Dataset

Datasets (training ratio)	UCLand(80%)	UCLand(50%)	NWPU(80%)	NWPU(20%)
MartaGAN	94.86 \pm 0.80	85.51 \pm 0.69	75.43 \pm 0.28	75.03 \pm 0.28
AttentionGAN	97.69\pm0.6	89.06 \pm 0.50	—	77.99 \pm 0.19
StyleGAN2+ADA	95.71 \pm 0.42	89.05 \pm 0.33	82.40 \pm 0.17	76.16 \pm 0.23
Ours	97.33 \pm 0.39	92.72\pm0.22	84.82\pm0.42	80.35\pm0.13

Table 5 Comparison of Quality Scores (FID \downarrow , KID \downarrow) on the UCLand, NWPU-RESISC45 and PatternNet Dataset

Methods	UCLand		NWPU		PN	
	FID	KID	FID	KID	FID	KID
MSGAN	137.52	53.66	83.55	38.35	122.68	44.76
TC-GAN	80.14	35.29	35.26	15.86	49.25	20.03
ContraGAN	133.91	54.62	117.29	50.76	122.55	50.18
BigGAN	144.66	61.24	89.29	40.62	132.35	55.29
StyleGAN2+DivCo	145.51	60.82	90.16	40.88	135.61	55.33
StyleGAN2+ADA	143.41	60.74	83.40	36.29	120.20	51.28
Our Method	64.33	30.29	18.33	6.33	30.35	11.28

**Fig. 10** Experiment results of class-conditional generation on the UC-Merced Dataset. StyleGAN2+ADA (Karras et al., 2020a) and MSGAN (Mao et al., 2019) have mode collapse problem, and they keep producing the same images for each class. In contrast, our method sidesteps this problem and generates a variety of images for each class.

conditional methods, our method do not use the label information directly, thus our class-conditional generation approach during inference process is different from other methods. The labels of our generated images are not consistent with those of training dataset. For example, the airport class corresponds to label "1" in the training dataset, while the label "1" correspond to the

Table 6 Ablation Study on Relationship Matrix C

Methods	UCLand	NWPU	PatternNet
Baseline	70.89	14.38	25.87
K-means(20)	68.22	13.31	24.78
K-means(40)	69.28	12.79	24.13
learnable(SimCLR)	66.77	12.14	23.01
learnable(CLIP)	66.98	12.01	23.08
learnable(ResNet)	67.01	12.12	23.11

Table 7 Ablation Study on Features from Different Blocks

Block	4	6	8	10	12
FID	15.92	15.05	10.89	17.23	22.19

river class in the generated images. We use pre-trained classification model ResNET50 to re-assign the labels of generated images. Then we use the new labels to control the generated images. In Fig.10, we observe that the compared models, MSGAN and StyleGAN2+ADA, suffer from mode collapse on the RS datasets, while our method generates diverse images. Next, we provide a quantitative comparison with well-established baselines: MSGAN, TC-GAN, DivCo, ContraGAN, conditional BigGAN and StyleGAN2. The experimental results are shown in the Table 5. Our method outperforms the compared methods as they all suffer from the mode

collapse problem. These empirical results confirm the efficacy of our approach. More visual results are available in the Appendix.

6.4 Ablation Study

In this section, we provide further ablation and analysis over different components of our method. More ablation experiments are available in the Appendix.

Relationship Matrix C . For the unsupervised generation, we provide several different methods to construct relationship matrix C . The first kind is based on SimCLR and K-means. We use the pre-trained SimCLR model to extract the features of RS data and then cluster these features using K-means. The resulting clustering centroids serve as prototypes of the training data. In this experiment we choose 20 and 40 clustering centroids, respectively. The second kind is the learnable matrix proposed in this paper. We choose SimCLR, CLIP (Radford et al., 2021), and ResNet50 (pretrained on the ImageNet) as the pre-trained encoder. Table 6 shows the results of the ablation study on UCLand, NWPU-RESISC45 and PatternNet datasets. We can observe that the choice of the pre-trained encoder has little impact on the results. In the following experiments, we choose the learnable approach and the SimCLR model as the pre-trained encoder.

Representations Z . For the unsupervised generation, we conduct ablation studies on features from different network layers. As different network layers are related to different levels of details in the generated image, and the earlier blocks of the network impact the coarse structure or content of the image. We conduct experiments on NWPU-RESISC45 dataset with StyleGAN2+ADA model, which consists of 14 blocks. We choose 5 blocks for comparison, and the results are shown in Table 10. We empirically choose the outputs of 8th block as the representations Z .

7 Conclusion

In this study, we aim to address the challenges posed by remote sensing (RS) images in the context of generative adversarial networks (GANs). We observe that RS images exhibit lower intrinsic dimensions compared to natural images, resulting in difficulties for the discriminator and an increased risk of overfitting. To tackle these issues, we propose an information-theoretic measure to capture the real data manifold and introduce manifold alignment regularization to effectively constrain the discriminator and improve the generator’s performance. We present novel learning paradigms for

both supervised and unsupervised RS image generation tasks, and establish a unified GAN framework. The efficacy of our method is validated through theoretical analysis and extensive experiments conducted on three RS datasets and three natural datasets, demonstrating the versatility and effectiveness of our approach.

Data Availability

The benchmark datasets can be downloaded from the literature cited in Subsubsection 6.

Conflict of interest

The authors declare no conflict of interest.

References

- Arjovsky M, Chintala S, Bottou L (2017) Wasserstein GAN. arXiv e-prints arXiv:1701.07875, 1701.07875
- Bang D, Shim H (2021) Mggan: Solving mode collapse using manifold-guided training. In: Proceedings of the IEEE/CVF international conference on computer vision, pp 2347–2356
- Bejiga MB, Hoxha G, Melgani F (2020) Improving text encoding for retro-remote sensing. IEEE Geoscience and Remote Sensing Letters 18(4):622–626
- Bell-Kligler S, Shocher A, Irani M (2019) Blind super-resolution kernel estimation using an internal-gan. Advances in Neural Information Processing Systems 32
- Bińkowski M, Sutherland DJ, Arbel M, Gretton A (2018) Demystifying mmd gans. In: International Conference on Learning Representations
- Brock A, Donahue J, Simonyan K (2018) Large scale gan training for high fidelity natural image synthesis. In: International Conference on Learning Representations
- Chen H, Li W, Shi Z (2021) Adversarial instance augmentation for building change detection in remote sensing images. IEEE Transactions on Geoscience and Remote Sensing 60:1–16
- Chen X, Chen S, Xu T, Yin B, Peng J, Mei X, Li H (2020) Smapgan: Generative adversarial network-based semisupervised styled map tile generation method. IEEE Transactions on Geoscience and Remote Sensing 59(5):4388–4406
- Cover T, Thomas JA (2006) Elements of information theory

- Esser P, Rombach R, Ommer B (2021) Taming transformers for high-resolution image synthesis. In: Proceedings of the IEEE/CVF conference on computer vision and pattern recognition, pp 12873–12883
- Gong C, Han J, Lu X (2017) Remote sensing image scene classification: Benchmark and state of the art. *Proceedings of the IEEE* 105(10):1865–1883
- Goodfellow IJ, Pouget-Abadie J, Mirza M, Xu B, Warde-Farley D, Ozair S, Courville A, Bengio Y (2014) Generative adversarial nets. In: Proceedings of the 27th International Conference on Neural Information Processing Systems - Volume 2, MIT Press, Cambridge, MA, USA, NIPS'14, p 2672–2680
- Gulrajani I, Ahmed F, Arjovsky M, Dumoulin V, Courville AC (2017) Improved training of wasserstein gans. *Advances in neural information processing systems* 30
- He J, Shi W, Chen K, Fu L, Dong C (2022) Gcfsr: a generative and controllable face super resolution method without facial and gan priors. In: Proceedings of the IEEE/CVF Conference on Computer Vision and Pattern Recognition, pp 1889–1898
- Heusel M, Ramsauer H, Unterthiner T, Nessler B, Hochreiter S (2017) Gans trained by a two time-scale update rule converge to a local nash equilibrium. *Advances in neural information processing systems* 30
- Jiang K, Wang Z, Yi P, Wang G, Lu T, Jiang J (2019) Edge-enhanced gan for remote sensing image super-resolution. *IEEE Transactions on Geoscience and Remote Sensing* 57(8):5799–5812
- Jiang L, Dai B, Wu W, Loy CC (2021a) Deceive d: Adaptive pseudo augmentation for gan training with limited data. *Advances in Neural Information Processing Systems* 34:21655–21667
- Jiang Y, Chang S, Wang Z (2021b) Transgan: Two pure transformers can make one strong gan, and that can scale up. *Advances in Neural Information Processing Systems* 34:14745–14758
- Kang M, Park J (2020) Contragan: Contrastive learning for conditional image generation. *Advances in Neural Information Processing Systems* 33:21357–21369
- Karras T, Laine S, Aila T (2019) A style-based generator architecture for generative adversarial networks. In: Proceedings of the IEEE/CVF conference on computer vision and pattern recognition, pp 4401–4410
- Karras T, Aittala M, Hellsten J, Laine S, Lehtinen J, Aila T (2020a) Training generative adversarial networks with limited data. *Advances in Neural Information Processing Systems* 33:12104–12114
- Karras T, Laine S, Aittala M, Hellsten J, Lehtinen J, Aila T (2020b) Analyzing and improving the image quality of stylegan. In: Proceedings of the IEEE/CVF conference on computer vision and pattern recognition, pp 8110–8119
- Khayatkhoei M, Singh MK, Elgammal A (2018) Disconnected manifold learning for generative adversarial networks. *Advances in Neural Information Processing Systems* 31
- Krizhevsky A, Hinton G (2009) Learning multiple layers of features from tiny images. *Handbook of Systemic Autoimmune Diseases* 1(4)
- Ledig C, Theis L, Huszár F, Caballero J, Cunningham A, Acosta A, Aitken A, Tejani A, Totz J, Wang Z, et al. (2017) Photo-realistic single image super-resolution using a generative adversarial network. In: Proceedings of the IEEE conference on computer vision and pattern recognition, pp 4681–4690
- Li Q, Kailkhura B, Anirudh R, Zhou Y, Liang Y, Varshney P (2018) Mr-gan: Manifold regularized generative adversarial networks. *arXiv preprint arXiv:181110427*
- Li T, Li Z, Rockwell H, Farimani A, Lee TS (2022) Prototype memory and attention mechanisms for few shot image generation. In: Proceedings of the Eleventh International Conference on Learning Representations, vol 18
- Lin D, Fu K, Wang Y, Xu G, Sun X (2017) Marta gans: Unsupervised representation learning for remote sensing image classification. *IEEE Geoscience and Remote Sensing Letters* 14(11):2092–2096, DOI 10.1109/LGRS.2017.2752750
- Ling H, Kreis K, Li D, Kim SW, Torralba A, Fidler S (2021) Editgan: High-precision semantic image editing. *Advances in Neural Information Processing Systems* 34:16331–16345
- Liu B, Zhu Y, Song K, Elgammal A (2020) Towards faster and stabilized gan training for high-fidelity few-shot image synthesis. In: International Conference on Learning Representations
- Liu R, Ge Y, Choi CL, Wang X, Li H (2021) Divco: Diverse conditional image synthesis via contrastive generative adversarial network. In: Proceedings of the IEEE/CVF Conference on Computer Vision and Pattern Recognition, pp 16377–16386
- Mao Q, Lee HY, Tseng HY, Ma S, Yang MH (2019) Mode seeking generative adversarial networks for diverse image synthesis. In: Proceedings of the IEEE/CVF conference on computer vision and pattern recognition, pp 1429–1437
- Mescheder L, Geiger A, Nowozin S (2018) Which training methods for gans do actually converge? In: International conference on machine learning, PMLR, pp 3481–3490
- Metz L, Poole B, Pfau D, Sohl-Dickstein J (2017) Unrolled generative adversarial networks. In: International Conference on Learning Representations

- Miyato T, Kataoka T, Koyama M, Yoshida Y (2018) Spectral Normalization for Generative Adversarial Networks. arXiv e-prints arXiv:1802.05957, [1802.05957](#)
- Mroueh Y, Sercu T (2017) Fisher gan. *Advances in neural information processing systems* 30
- Ni Y, Koniusz P, Hartley R, Nock R (2022) Manifold learning benefits gans. In: *Proceedings of the IEEE/CVF Conference on Computer Vision and Pattern Recognition*, pp 11265–11274
- Pan X, Tewari A, Leimkühler T, Liu L, Meka A, Theobalt C (2023) Drag your gan: Interactive point-based manipulation on the generative image manifold. arXiv preprint arXiv:230510973
- Park N, Anand A, Moniz JRA, Lee K, Chakraborty T, Choo J, Park H, Kim Y (2017) Mmgan: Manifold matching generative adversarial network. arXiv preprint arXiv:170708273
- Park T, Liu MY, Wang TC, Zhu JY (2019) Semantic image synthesis with spatially-adaptive normalization. In: *Proceedings of the IEEE/CVF conference on computer vision and pattern recognition*, pp 2337–2346
- Patashnik O, Wu Z, Shechtman E, Cohen-Or D, Lischinski D (2021) Styleclip: Text-driven manipulation of stylegan imagery. In: *Proceedings of the IEEE/CVF International Conference on Computer Vision*, pp 2085–2094
- Radford A, Kim JW, Hallacy C, Ramesh A, Goh G, Agarwal S, Sastry G, Askell A, Mishkin P, Clark J, et al. (2021) Learning transferable visual models from natural language supervision. In: *International conference on machine learning*, PMLR, pp 8748–8763
- Richardson E, Alaluf Y, Patashnik O, Nitzan Y, Azar Y, Shapiro S, Cohen-Or D (2021) Encoding in style: a stylegan encoder for image-to-image translation. In: *Proceedings of the IEEE/CVF conference on computer vision and pattern recognition*, pp 2287–2296
- Rui X, Cao Y, Yuan X, Kang Y, Song W (2021) Disastergan: Generative adversarial networks for remote sensing disaster image generation. *Remote Sensing* 13(21), DOI [10.3390/rs13214284](#)
- Salimans T, Goodfellow I, Zaremba W, Cheung V, Radford A, Chen X (2016) Improved techniques for training gans. In: *Proceedings of the 30th International Conference on Neural Information Processing Systems*, Curran Associates Inc., Red Hook, NY, USA, NIPS'16, p 2234–2242
- Shahbazi M, Danelljan M, Paudel DP, Gool LV (2022) Collapse by conditioning: Training class-conditional GANs with limited data. In: *International Conference on Learning Representations*
- Srivastava A, Valkov L, Russell C, Gutmann MU, Sutton C (2017) Veegan: Reducing mode collapse in gans using implicit variational learning. *Advances in neural information processing systems* 30
- Tseng HY, Jiang L, Liu C, Yang MH, Yang W (2021) Regularizing generative adversarial networks under limited data. In: *Proceedings of the IEEE/CVF Conference on Computer Vision and Pattern Recognition*, pp 7921–7931
- Wang SY, Bau D, Zhu JY (2021) Sketch your own gan. In: *Proceedings of the IEEE/CVF International Conference on Computer Vision*, pp 14050–14060
- Wei Y, Luo X, Hu L, Peng Y, Feng J (2020) An improved unsupervised representation learning generative adversarial network for remote sensing image scene classification. *Remote Sensing Letters* 11(6):598–607
- Xiong Y, Guo S, Chen J, Deng X, Sun L, Zheng X, Xu W (2020) Improved srgan for remote sensing image super-resolution across locations and sensors. *Remote Sensing* 12(8):1263
- Xu L, Jordan MI (1996) On convergence properties of the em algorithm for gaussian mixtures. *Neural computation* 8(1):129–151
- Xu Q, Huang G, Yuan Y, Guo C, Sun Y, Wu F, Weinberger KQ (2018) An empirical study on evaluation metrics of generative adversarial networks. arXiv preprint arXiv:180607755
- Yang C, Shen Y, Xu Y, Zhou B (2021) Data-efficient instance generation from instance discrimination. *Advances in Neural Information Processing Systems* 34:9378–9390
- Yang Y, Newsam S (2010) Bag-of-visual-words and spatial extensions for land-use classification. In: *Proceedings of the 18th SIGSPATIAL international conference on advances in geographic information systems*, pp 270–279
- Yu F, Seff A, Zhang Y, Song S, Funkhouser T, Xiao J (2015) Lsun: Construction of a large-scale image dataset using deep learning with humans in the loop. arXiv preprint arXiv:150603365
- Yu Y, Li X, Liu F (2019) Attention gans: Unsupervised deep feature learning for aerial scene classification. *IEEE Transactions on Geoscience and Remote Sensing* 58(1):519–531
- Zhang H, Goodfellow I, Metaxas D, Odena A (2019a) Self-attention generative adversarial networks. In: *International conference on machine learning*, PMLR, pp 7354–7363
- Zhang H, Zhang Z, Odena A, Lee H (2019b) Consistency regularization for generative adversarial networks. In: *International Conference on Learning Representations*

- Zhao B, Zhang S, Xu C, Sun Y, Deng C (2021) Deep fake geography? when geospatial data encounter artificial intelligence. *Cartography and Geographic Information Science* 48(4):338–352
- Zhao S, Liu Z, Lin J, Zhu JY, Han S (2020) Differentiable augmentation for data-efficient gan training. *Advances in Neural Information Processing Systems* 33:7559–7570
- Zhou W, Newsam S, Li C, Shao Z (2018) Patternnet: A benchmark dataset for performance evaluation of remote sensing image retrieval. *ISPRS journal of photogrammetry and remote sensing* 145:197–209

This appendix first shows more results of the motivating experiments. Second, we introduce the experiment setup and conduct more ablation studies on our method. Finally, we present additional visual results of our method compared with the state-of-the-art models.

A Motivating Experiments

To illustrate the overfitting problem of the discriminator on remote sensing (RS) data, we conduct the same experiments as Fig.1 (in the main paper) on PatternNet (PN) dataset. We randomly sample 30,000 images from the PN and FFHQ256 datasets, respectively. The training curves of StyleGAN2 are shown in Fig.11(a). The GAN model still diverges earlier on PN dataset than FFHQ256 dataset. In Fig.11(b), we show the outputs of the discriminator during training. The experiment results further prove our finding that the overfitting problem of the discriminator is more severe on RS data. We also conduct the same experiments as Fig.2 (in the main paper) on PN dataset. The results are shown in Fig.12, which are consistent with the main paper.

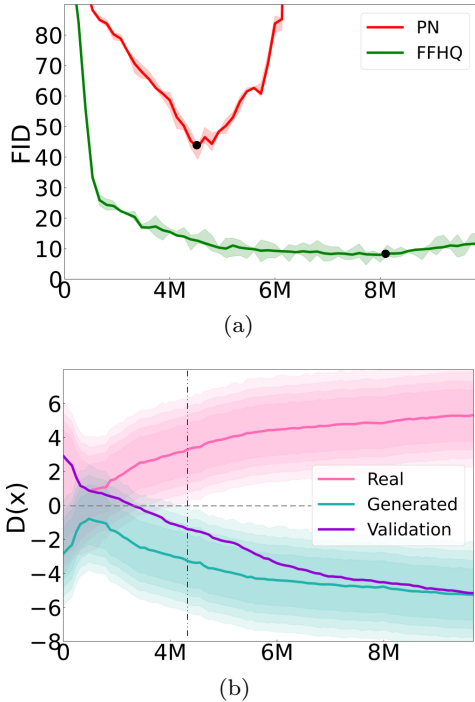


Fig. 11 The horizontal axis indicates the training process (the number of real images shown to the discriminator). (a) Training curves of StyleGAN2 on PN and FFHQ datasets. We randomly sample 30,000 training images from these two datasets, respectively. (b) The outputs of the discriminator during training on PN dataset.

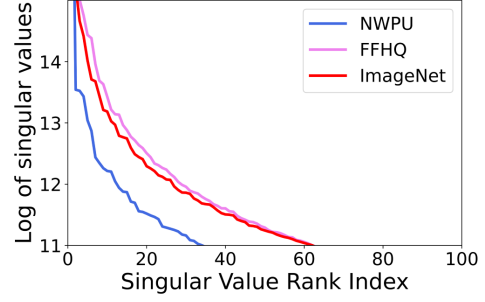


Fig. 12 Singular value decomposition on PN dataset and natural images in sorted order and logarithmic scale.

Table 8 Ablation Study on Regularizing Generator vs. Discriminator.

Methods	UCLand	NWPU	PN
Baseline	70.89	14.38	25.87
Only G	69.95	12.85	25.06
Only D	67.23	12.44	24.83
Ours	66.98	12.04	23.01

B Experiment Setup

B.1 Datasets

We use three remote sensing datasets to evaluate our method: the UC Merced Land Use (UCLand) Dataset, NWPU-RESISC45 (NWPU) Dataset and PatternNet (PN) Dataset.

The UC Merced Land Use Dataset is one of the most widely used datasets in the field of remote sensing scene classification. It has 21 scene categories, each with 100 images. Each image has the size 256×256 and a spatial resolution of 0.3m. The images in the dataset come from more than 20 cities in the United States, including Las Vegas, Los Angeles, Miami, Santa Barbara, and Seattle.

The NWPU-RESISC45 Dataset has 31,500 images covering more than 100 countries and regions around the world. It has 45 categories with 700 images in each category. Each image is 256×256 pixels in size. The spatial resolution of this dataset is up to 0.2m and the lowest is 30m. In addition, the images are varied in lighting, shooting angle, imaging conditions, and so on.

The PatternNet Dataset is a large-scale high-resolution remote sensing dataset. It has 38 categories with 800 images in each category. Each image is 256×256 pixels in size. The spatial resolution of this dataset varies from 0.06m per pixel to 4.7m per pixel. The images in PatternNet are collected from Google Earth imagery or via the Google Map API for some US cities.

B.2 More Ablation Study

Regularizing generator vs. discriminator.. For the unsupervised generation, our default method add regularization on the loss functions of both generator G and discriminator D . In this experiment, we investigate the effectiveness of separately regularizing G and D . Table 8 presents the results of

Table 9 Ablation Study on the Hyperparameter λ

λ	UCLand	NWPU	PN
0.1	70.60	14.93	25.09
0.5	69.43	14.91	24.92
0.7	68.55	13.68	24.81
1	66.98	12.04	23.01
3	70.22	14.31	24.78

Table 10 Ablation Study on the Hyperparameter γ

γ	UCLand	NWPU	PN
0.1	72.29	13.87	26.13
0.5	70.62	14.16	25.22
0.7	71.09	14.33	23.92
1	66.98	12.04	23.01
3	71.24	15.09	26.07

Table 11 Ablation Study on the Hyperparameter β

β	UCLand	NWPU	PN
0.1	71.35	14.62	25.38
0.5	71.32	14.69	24.57
0.7	69.23	14.24	25.32
1	66.98	12.04	23.01
3	70.93	15.88	24.74

the ablation study on UCLand, NWPU-RESISC45 and PatternNet datasets. The No Regularization version yields poor results as expected. Adding the regularization method on D already brings significant improvement to the model under different datasets. As proposed in our final method, adding the regularization on both G and D achieves the best results.

Hyperparameters. For the unsupervised generation, we conduct the ablation study on the hyperparameters λ , γ and β using TC-GAN+MAC on UCLand, NWPU-RESISC45 and PatternNet datasets. The FID scores are shown in Table 9, Table 10, Table 11. Based on the experiment results, we set $\lambda = 1$, $\gamma = 1$ and $\beta = 1$ in the following experiments. For the class-conditional generation, we use the same hyperparameters $\lambda = 1$, $\gamma = 1$ as the unsupervised generation.

B.3 Unsupervised Generation Results

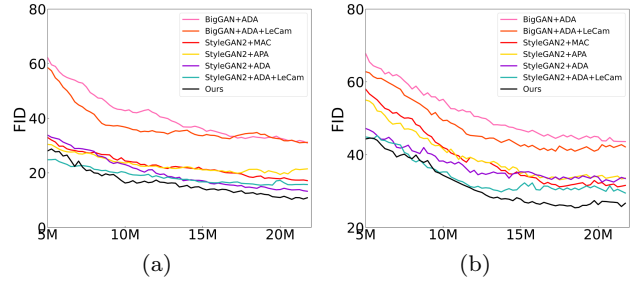
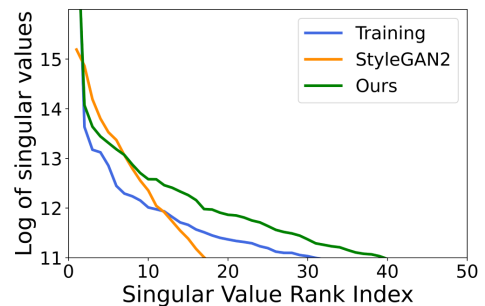
We first show the training curves of our experiments on NWPU and PN datasets in Fig.13. Compared with the well-established models, our method not only alleviates the overfitting problem of the discriminator, but also gets better quality scores. As depicted in Fig.14, we also compare the singular values of the images generated by StyleGAN2+ADA and our proposed method on PN dataset. The results are consistent with the main paper.

Moreover, we split the training classes into three categories: **small**, **medium**, **large**, according to the proportion of artificial landscapes. The categories are shown in Table.12,

Table 12 Three Categories on the UCLand Dataset

Category	Classes
small	beach,forest,river,chaparral
medium	baseball diamond, freeway, golf course, sparse residential
large	agricultural, airplane, buildings, dense residential, harbor, intersection, medium residential, mobile home park, overpass, parking lot, runway, storage tanks, tennis court

Table.13 and Table.14, and we can observe that these categories are distributed non-uniformly on the PN and UCLand datasets. Then, we train the classification model ResNET50 on the training datasets and classify the generated images into the three categories. The visual results are shown in Fig.15, Fig.16 and Fig.17, respectively. Our method is based on StyleGAN2+ADA. On the UCLand and PN datasets, the compared models learn the biased distribution and produce more artificial landscapes. On the NWPU datasets, the compared models tend to produce more natural landscapes, although the distribution of the three categories are almost uniform on this dataset. In comparison, our method produces a more even distribution of natural and artificial landscapes, which further prove that our method can learn the real data manifold of the RS data.

**Fig. 13** (a) Training curves on NWPU dataset. (b) Training curves on PN dataset.**Fig. 14** Singular value decomposition on PN dataset, generated images by StyleGAN2, and generated images by our method in sorted order and logarithmic scale.

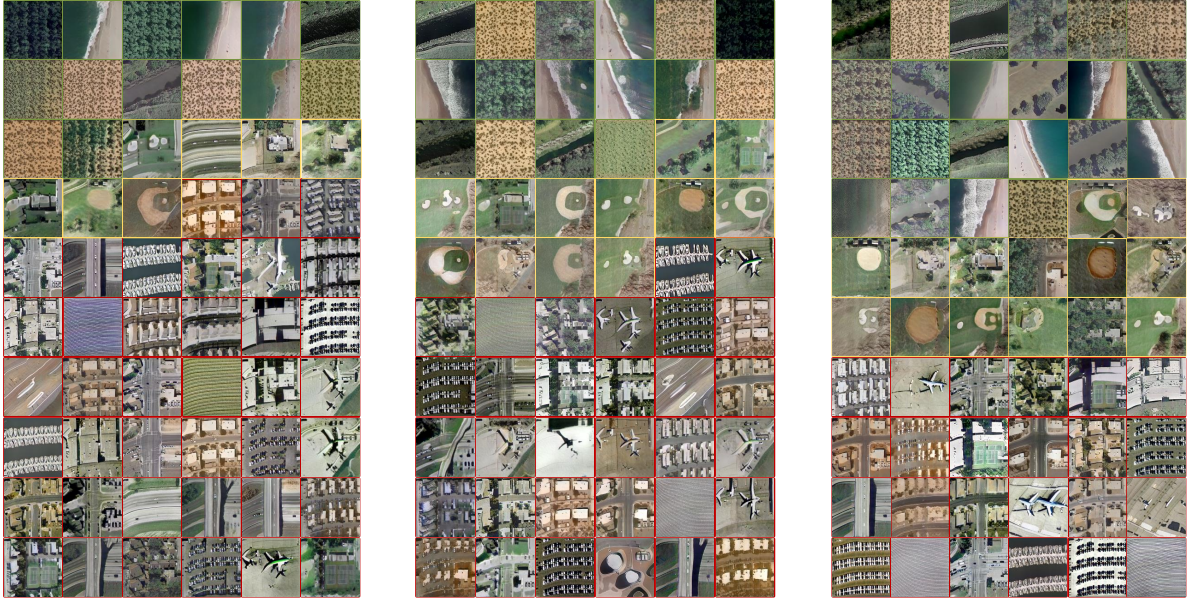


Fig. 15 Random Samples from BigGAN+ada (left), Stylegan2+ada (middle) and our method (right) trained on the UCLand Dataset.

Table 13 Three Categories on the NWPU-RESISC45 Dataset

Category	Classes
small	beach,forest,river,chaparral, cloud, desert, island, lake, meadow, mountain, sea ice, snowberg, wetland
medium	baseball diamond, freeway, golf course, sparse residential, basketball court, bridge, circular farmland, medium residential, rectangular farmland, ship, terrace, tennis court
large	airport, airplane, dense residential, harbor, roundabout, stadium, intersection, mobile home park, overpass, palace, railway, railway station, thermal power station, parking lot, runway, storage tanks, church, commercial area, ground track field, industrial area

Table 14 Three Categories on the PatternNet Dataset

Category	Classes
small	beach,forest,river,chaparral
medium	baseball field, cemetery, christmas tree farm, freeway, football field, golf course, sparse residential, basketball court, bridge, oil gas field, oil well, tennis court, transformer station
large	airplane, dense residential, closed road, harbor, ferry terminal, coastal mansion, crosswalk, intersection, mobile home park, nursing home, overpass, railway, parking lot, parking space, runway, runway marking, shipping yard, solar panel, swimming pool, storage tanks, wastewater treatment plant

B.4 Class-conditional Generation Results

The visual results of class-conditional generation are shown in Fig.18, Fig.19 and Fig.20, respectively.

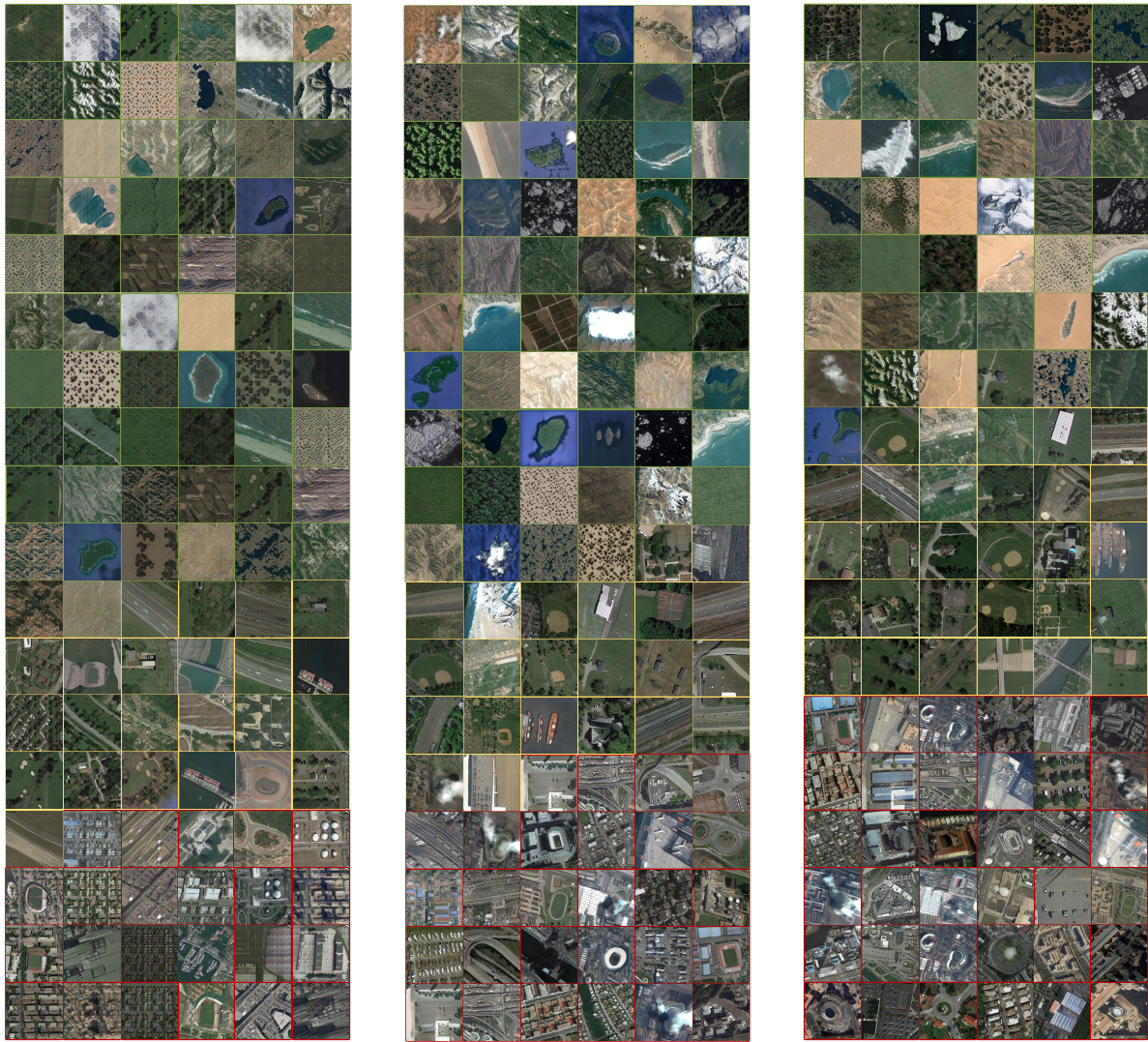


Fig. 16 Random Samples from BigGAN+ada (left), Stylegan2+ada (middle) and our method (right) trained on the NWPU Dataset.

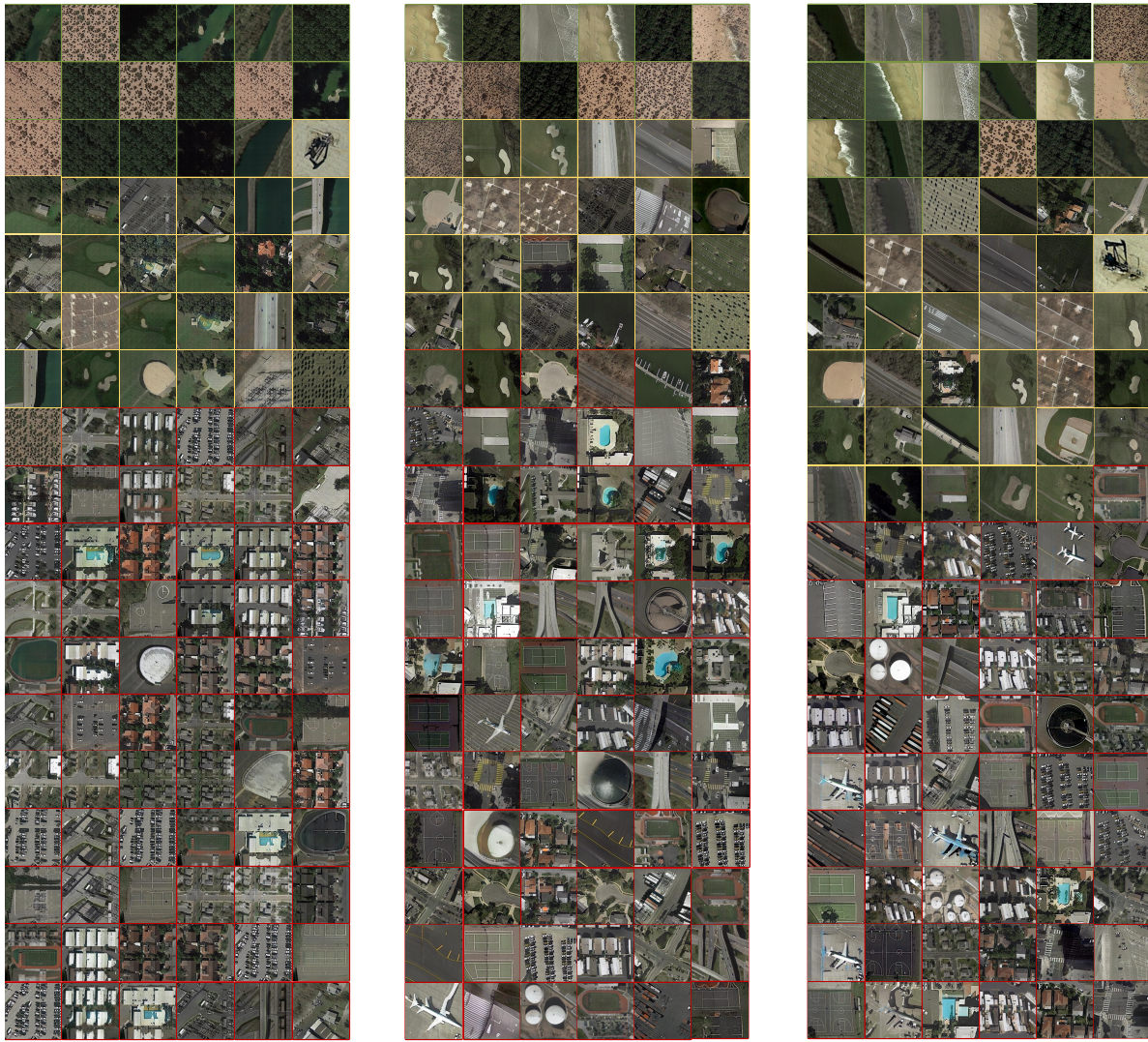


Fig. 17 Random Samples from BigGAN+ada (left), Stylegan2+ada (middle) and our method (right) trained on the PN Dataset.

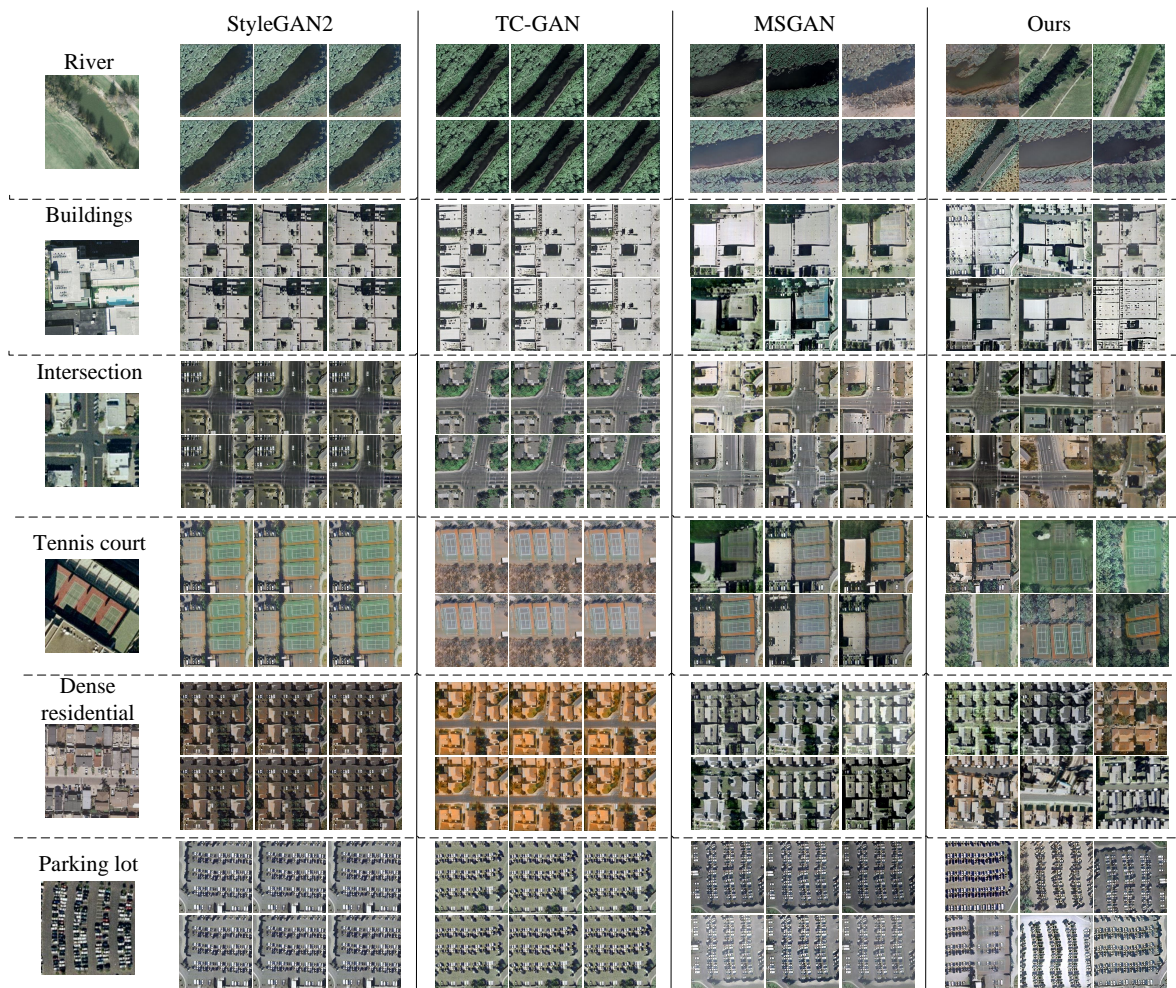


Fig. 18 Experiment results of class-conditional generation on the UCLand Dataset.

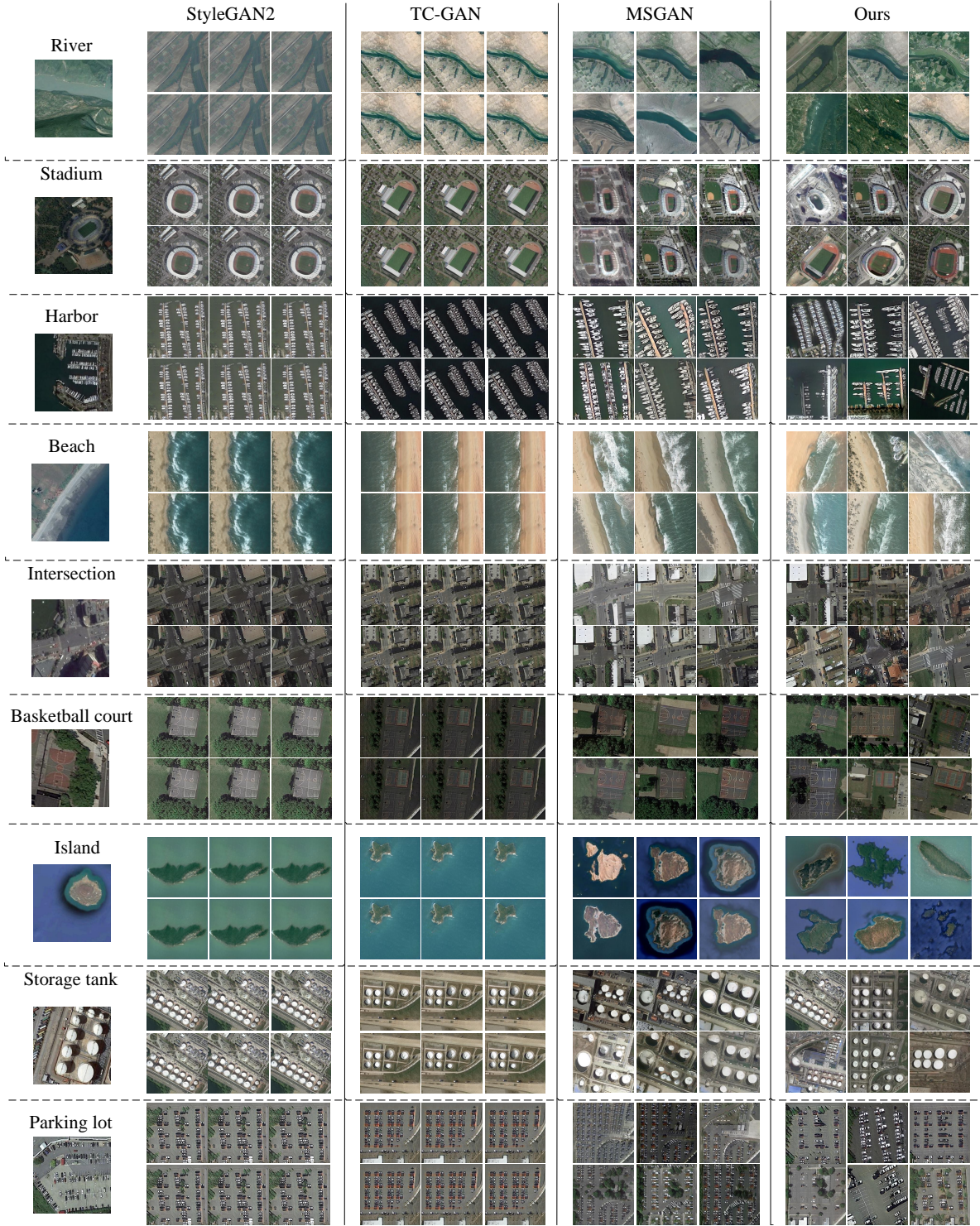


Fig. 19 Experiment results of class-conditional generation on the NWPU Dataset.

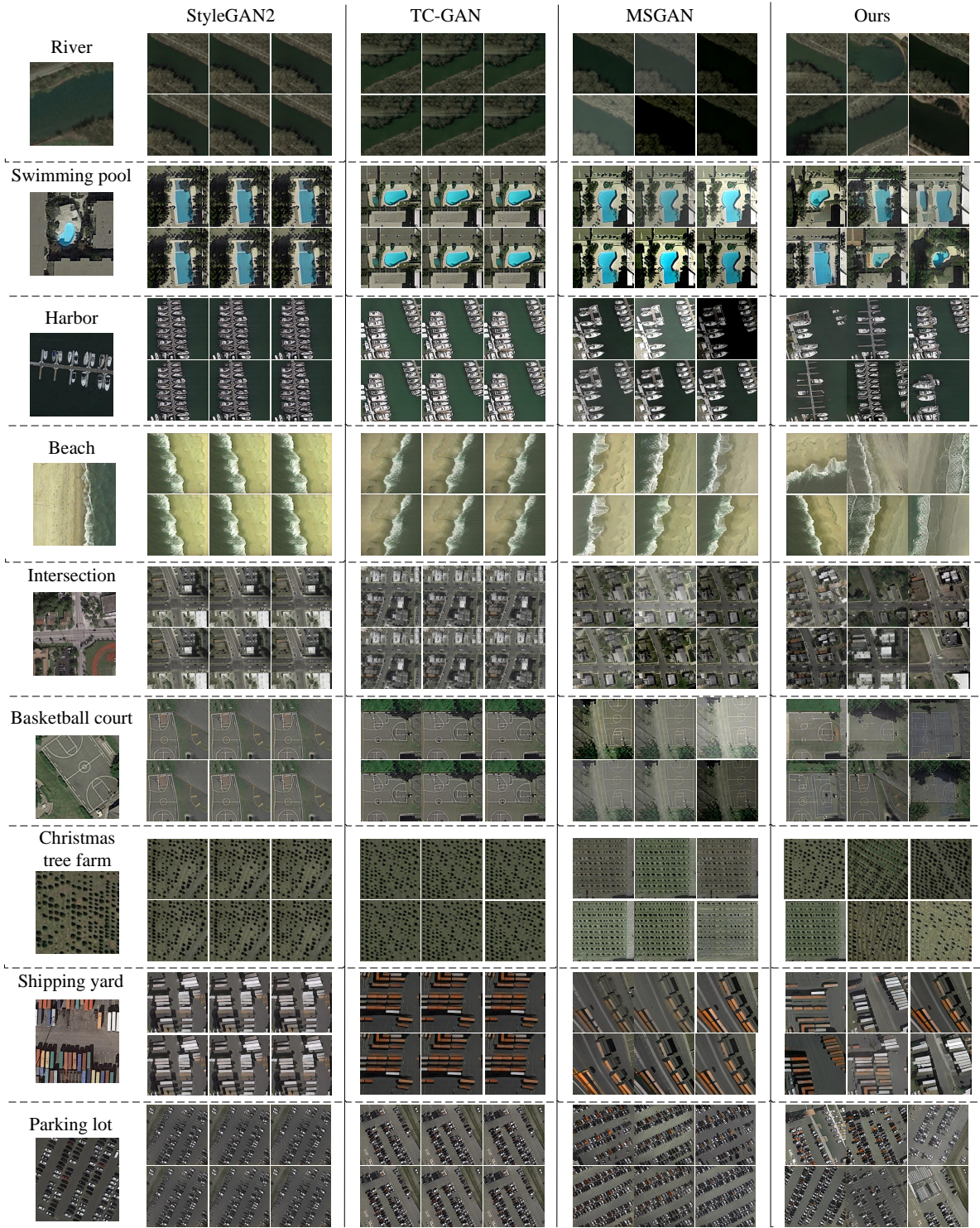


Fig. 20 Experiment results of class-conditional generation on the PN Dataset.